

Influence of scattering effects on the interaction between longitudinal modes in laser diodes

Eduard Kuhn¹, Angela Thränhardt²

submitted: August 18, 2023

¹ Weierstrass Institute
Mohrenstr. 39
10117 Berlin
Germany
E-Mail: eduard.kuhn@wias-berlin.de

² Technische Universität Chemnitz
Institute of Physics
Reichenhainerstr. 70
09126 Chemnitz
Germany
E-Mail: angela.thraenhardt@physik.tu-chemnitz.de

No. 3038
Berlin 2023



2010 *Physics and Astronomy Classification Scheme*. 42.55.Px.

Key words and phrases. Laser diode, mode interaction, mode competition, nitride laser diode.

This work was performed in the frame of the German Leibniz Association funded project PCSElence (K487/2022).

Edited by
Weierstraß-Institut für Angewandte Analysis und Stochastik (WIAS)
Leibniz-Institut im Forschungsverbund Berlin e. V.
Mohrenstraße 39
10117 Berlin
Germany

Fax: +49 30 20372-303
E-Mail: preprint@wias-berlin.de
World Wide Web: <http://www.wias-berlin.de/>

Influence of scattering effects on the interaction between longitudinal modes in laser diodes

Eduard Kuhn, Angela Thränhardt

Abstract

A predictive model of scattering processes in semiconductor lasers is derived, enabling us to model relaxation processes starting from well-known parameters such as the dielectric constant. The resulting effective mode interaction terms are explicitly calculated for an (InGa)N quantum well using Coulomb scattering. In contrast to the method used so far to model mode competition phenomena in Fabry-Pérot type laser diodes, the model correctly includes e.g. accelerated scattering at higher densities or temperatures and eliminates the scattering rate as an unknown parameter. The effective mode interaction term derived in this work can be used for the simulation of the mode dynamics in various laser diode types, for example broad area laser diodes, where multiple transversal and longitudinal modes are active. Thus, our model offers an increased predictability and improved modelling of switch-on behavior.

1 Introduction

Fabry-Pérot type laser diodes are used for various applications such as laser displays [1–4] and projection [5–7], showing mode-competition phenomena [8, 9]. For example, these lasers show mode hopping, where the level of activity of different longitudinal modes changes over time due to an anti-symmetric interaction of the modes. In a more recent development, a similar effect has been observed in broad area laser diodes, specifically in the presence of multiple lateral modes [10]. This kind of mode interaction can be explained by beating vibrations of the carrier densities in the quantum well that appear when multiple longitudinal modes are active at the same time [11].

The most common way to simulate the mode dynamics is to use rate equations, i.e. to formulate equations of motion for the photon numbers of all relevant modes and the carrier density. An alternative method is the traveling wave method, where a partial differential equation for the electrical field is solved [12–18]. However, up to this point, no mode dynamics simulations using the traveling wave method have been able to qualitatively replicate the experimental results.

When using rate equations, the state of the charge carriers is usually described by the total number of carriers in the quantum well not specifying their spatial momentum or energy distribution. In order to describe effects such as spatial or spectral hole burning a more detailed description is needed. One possibility is to use a spatially varying carrier density or even to use electron and hole distribution functions that determine the average occupation of the different energy levels [19].

The direct treatment of the beating vibrations of the quantum well carriers is computationally expensive, as the period of the vibrations is typically in the region of a few picoseconds [20] but the mode competition effects occur on the timescale of 100 ns [21]. The computation time can be significantly reduced by using an effective mode interaction term in the rate equations instead. This effective term describes the interaction between different optical modes and it is no longer necessary to consider

the beating vibrations of the quantum well carriers in the calculations. The equations of motion of the photon numbers in each mode are expanded by adding an additional mode interaction term where the strength of the interaction is determined by the frequency difference of two modes. This effective interaction term was derived for maser devices by Lamb et al. [22] and for Fabry-Pérot laser diodes with a single lateral mode by Yamada et al. using a constant scattering time [11, 23–27].

In section 2 of this publication we derive these effective mode interaction terms using ab initio scattering terms, e.g. Coulomb scattering. This kind of scattering term has been used extensively in the literature to calculate optical properties such as the refractive index and absorption/gain spectra for different materials, e.g. for gallium arsenide [28–35] and also gallium nitride [36] based material systems. The derived effective mode interaction term is valid not only for narrow ridge laser diodes but also extends to broad ridge laser diodes exhibiting multiple lateral modes. This may be used to understand the streak camera observation as shown in Ref.[10]

In section 3 the effective mode interaction term is calculated for an (InGa)N quantum well using Coulomb scattering. Differences to a “traditional” calculation using a constant scattering time occur in particular for small frequency differences of the participating modes ($\Delta\omega < 1 \text{ ps}^{-1}$). The interaction term also depends strongly on the field strength at the quantum well or alternatively the photon density. The effect of the scattering terms on the mode dynamics using an effective mode interaction term is also studied for a simple example where the carrier densities were assumed to be constant.

2 Theory

2.1 Basic Theory

In order to simulate the mode dynamics of laser diodes we need to consider the equations of motion for the photon numbers S_p . These photon numbers are the absolute squares of the coefficients B_p in the expansion of the optical field $\mathbf{E}(\mathbf{r})$, $S_p = |B_p|^2$, and

$$\mathbf{E}(\mathbf{r}) = \sum_p i \sqrt{\frac{\hbar\omega_p}{2\epsilon_0}} [B_p \mathbf{u}_p(\mathbf{r}) - B_p^* \mathbf{u}_p^*(\mathbf{r})],$$

where $\mathbf{u}_p(\mathbf{r})$ are the respective photon mode functions, ω_p are the mode frequencies and ϵ_0 is the vacuum permittivity. The mode functions typically depend on the device geometry. For example, for Fabry-Pérot laser diodes they can be written as

$$\mathbf{u}_{pm} = g_p(y) \mathbf{t}_m(x, z),$$

where the index p is used for the longitudinal mode function $g_p(y)$ and m is used for the transversal mode function $\mathbf{t}_m(x, z)$. In the following these two indices are combined into a single index p . Here z is the growth direction, x is the lateral coordinate and y is the longitudinal coordinate.

The equation of motion for the coefficients B_p can be derived using the Heisenberg picture and is given by an integral of the mode function with the polarization \mathbf{P} of the quantum well [37]:

$$\begin{aligned} \frac{d}{dt} B_p &= -i\omega_p B_p + \sqrt{\frac{\omega_p}{2\hbar\epsilon_0}} \int d^3\mathbf{r} \mathbf{u}_p^*(\mathbf{r}) \mathbf{P}(\mathbf{r}, \omega_p) \\ \Rightarrow \frac{d}{dt} S_p &= \frac{d}{dt} |B_p|^2 = \sqrt{\frac{2\omega_p}{\hbar\epsilon_0}} \int d^3\mathbf{r} \text{Re} \{ B_p^* \mathbf{u}_p^*(\mathbf{r}) \cdot \mathbf{P}(\mathbf{r}, \omega_p) \} \end{aligned} \quad (1)$$

For the actual simulation of a laser device, additional terms are needed. For example terms that describe spontaneous emission and photon losses inside the cavity.

In the present model we also require a description of the carriers in the quantum well in order to calculate the polarization \mathbf{P} . For this purpose we use the Semiconductor Bloch equations [19, 38, 39], which are equations of motion for the carrier distribution functions $f_{\mathbf{k}}^e$, $f_{\mathbf{k}}^\lambda$ and microscopic polarizations $\psi_{\mathbf{k}}^\lambda$. These polarizations are used to describe optical transitions between the conduction and valence band and therefore indirectly couple the distribution functions with the optical field. A derivation of these equations for the space-dependent case is given in Ref. [19].

In order to calculate the changes of the distribution functions, the equations of motion for the microscopic polarizations $\psi_{\mathbf{k}}^\lambda$ need to be solved. These are given by [19, 38, 39]

$$\frac{d}{dt}\psi_{\mathbf{k}}^\lambda = i\Omega_{\mathbf{k}}^\lambda (1 - f_{\mathbf{k}}^\lambda - f_{\mathbf{k}}^e) - \frac{i}{\hbar} (\tilde{\varepsilon}_{\mathbf{k}}^e + \tilde{\varepsilon}_{\mathbf{k}}^\lambda) \psi_{\mathbf{k}}^\lambda + \left. \frac{d}{dt}\psi_{\mathbf{k}}^\lambda \right|_{\text{Scatter}}, \quad (2)$$

where the index λ is used to index the different hole bands and $f_{\mathbf{k}}^\lambda$ are the hole distribution functions. Here only one conduction band with the distribution function $f_{\mathbf{k}}^e$ is considered. Although all the quantities are dependent on x , y , and t , we have omitted these dependencies for brevity's sake. In this equation $\tilde{\varepsilon}_{\mathbf{k}}^\lambda$ are the Hartree-Fock energies

$$\tilde{\varepsilon}_{\mathbf{k}}^\lambda = \varepsilon_{\mathbf{k}}^\lambda - \frac{1}{A} \sum_{\mathbf{q}} V_{\mathbf{q}}^{\lambda\lambda} f_{\mathbf{k}+\mathbf{q}}^\lambda,$$

where A is the quantization area of the quantum well and $V_{\mathbf{q}}^{\lambda\lambda'}$ are the Coulomb matrix elements. In the rotating wave approximation (RWA) the Rabi frequency $\Omega_{\mathbf{k}}^\lambda$ is given by [37]:

$$\hbar\Omega_{\mathbf{k}}^\lambda = -\frac{e}{m_0} \sum_p \sqrt{\frac{\hbar}{2\omega_p \epsilon_0}} B_p \mathbf{p}_\lambda^* \cdot \mathbf{u}_p(\mathbf{r}_\parallel, z_{\text{QW}}) + \frac{1}{A} \sum_{\mathbf{q}} V_{\mathbf{q}}^{e\lambda} \psi_{\mathbf{k}+\mathbf{q}}^\lambda,$$

where m_0 is the electron mass, \mathbf{r}_\parallel is a shorthand logogram for the x and y coordinates and the quantum well is located at z_{QW} . The strength of the interaction with an optical field is determined by the momentum matrix element \mathbf{p}_λ and for a quantum well the Coulomb matrix element $V_{\mathbf{q}}^{\lambda\lambda'}$ is given by

$$V_{\mathbf{q}}^{\lambda\lambda'} = \frac{e^2}{2\epsilon_0 \epsilon_b q} \int dz \int dz' |\xi_\lambda(z)|^2 |\xi_{\lambda'}(z')|^2 e^{-|q(z-z')|},$$

where $\xi_\lambda(z)$ are the envelope functions of the different bands and ϵ_b is the dielectric function of the background. For the dephasing of the polarization due to carrier scattering, the term

$$\left. \frac{d}{dt}\psi_{\mathbf{k}}^\lambda \right|_{\text{Scatter}} = - \sum_{\mathbf{k}'} \frac{\Gamma_{\mathbf{k}\mathbf{k}'}^\lambda}{\hbar} \psi_{\mathbf{k}'}^\lambda, \quad (3)$$

is used. The exact form of the dephasing matrix $\Gamma_{\mathbf{k}\mathbf{k}'}^\lambda$ depends on the scattering processes that are considered. An example is given in the appendix for Coulomb scattering. The macroscopic polarization in Eq. (1) is parallel to the field and given by [37]

$$\mathbf{u}_p^*(\mathbf{r}) \cdot \mathbf{P}(\mathbf{r}, \omega_p) = -\delta(z - z_{\text{QW}}) u_p^*(\mathbf{r}_\parallel) \frac{iep_\lambda}{\omega_p m_0} \frac{2}{A} \sum_{\lambda\mathbf{k}} \psi_{\mathbf{k}}^\lambda(\mathbf{r}_\parallel), \quad (4)$$

where $u_p(\mathbf{r})$ is the mode function at the position of the quantum well:

$$\mathbf{p}_\lambda \cdot \mathbf{u}_p^*(\mathbf{r}_\parallel, z_{\text{QW}}) = p_\lambda u_p^*(\mathbf{r}_\parallel). \quad (5)$$

The equations of motion for the electron and hole distribution functions are

$$\begin{aligned} \frac{d}{dt} f_{\mathbf{k}}^e &= 2 \sum_{\lambda} \text{Im} \left\{ \psi_{\mathbf{k}}^{\lambda} (\Omega_{\mathbf{k}}^{\lambda})^* \right\} - \frac{f_{\mathbf{k}}^e}{\tau_{\text{nr}}} + \left. \frac{d}{dt} f_{\mathbf{k}}^e \right|_{\text{Scatter}}, \\ \frac{d}{dt} f_{\mathbf{k}}^h &= 2 \text{Im} \left\{ \psi_{\mathbf{k}}^{\lambda} (\Omega_{\mathbf{k}}^{\lambda})^* \right\} - \frac{f_{\mathbf{k}}^h}{\tau_{\text{nr}}} + \left. \frac{d}{dt} f_{\mathbf{k}}^h \right|_{\text{Scatter}}. \end{aligned} \quad (6)$$

Here, only terms that are relevant for the mode interaction are considered. The constant τ_{nr} is used to account for nonradiative losses. Further terms that are relevant in a laser simulation include the pumping of the quantum wells and losses due to spontaneous emission and Auger recombination.

The scattering term plays a crucial role in the relaxation of the system towards an equilibrium state, where the distribution functions can be described by Fermi-Dirac distributions. When the deviations of the distribution functions from the Fermi-Dirac form are small, the scattering term can be linearized as follows:

$$\left. \frac{d}{dt} f_{\mathbf{k}}^{\lambda} \right|_{\text{Scatter}} = - \sum_{\mathbf{k}'} J_{\mathbf{k}\mathbf{k}'}^{\lambda} \left(f_{\mathbf{k}'}^{\lambda} - f_{\mathbf{k}'}^{\lambda, \text{FD}} \right). \quad (7)$$

Here, $f_{\mathbf{k}}^{\lambda, \text{FD}}$ represents the Fermi-Dirac distributions at a fixed temperature, which yield the same density as $f_{\mathbf{k}}^{\lambda}$. The scattering matrix $J_{\mathbf{k}\mathbf{k}'}^{\lambda}$, similar to the dephasing matrix $\Gamma_{\mathbf{k}\mathbf{k}'}^{\lambda}$, depends on the specific scattering processes being considered. In the appendix, the scattering matrix for Coulomb scattering is provided. The simplest approximation for the scattering matrix assumes a constant scattering time τ_s :

$$J_{\mathbf{k}\mathbf{k}'}^{\lambda} = \frac{1}{\tau_s} \delta_{\mathbf{k}\mathbf{k}'}. \quad (8)$$

Using this approximation, the deviations from the Fermi-Dirac distributions decay exponentially:

$$\left. \frac{d}{dt} f_{\mathbf{k}}^{\lambda} \right|_{\text{Scatter}} = - \frac{f_{\mathbf{k}}^{\lambda} - f_{\mathbf{k}}^{\lambda, \text{FD}}}{\tau_s}.$$

2.2 Mode interaction term for a single lateral mode

Yamada et al. have provided a theoretical description of mode-competition phenomena in Fabry-Pérot laser diodes for narrow-ridge laser diodes with a single lateral mode [23]. In their rate equation model, they incorporate a mode interaction term expressed in terms of two matrices [26]:

$$\left. \frac{d}{dt} S_p \right|_{\text{Interaction}} = - \sum_{q \neq p} (D_{pq} + H_{pq}) S_q S_p.$$

This mode interaction arises due to the beating vibrations of carrier densities in the longitudinal direction, as illustrated in Fig. 1. The symmetric interaction matrix D_{pq} , which accounts for mode interaction, is given by:

$$D_{pq} = \frac{4}{3} \frac{B}{\left(\frac{2\pi c \tau_{\text{in}}}{\lambda_p^2} \right)^2 (\lambda_p - \lambda_q)^2 + 1}, \quad (9)$$

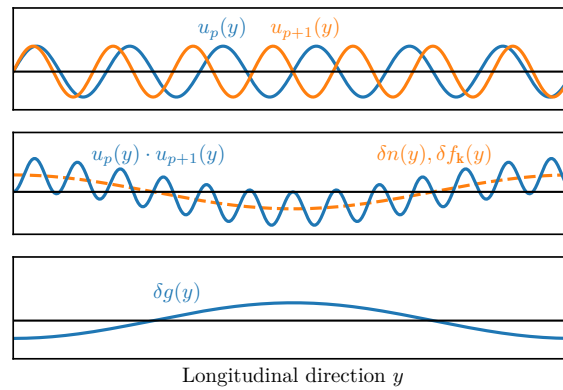


Figure 1: Illustration of the interaction of two active modes. When two longitudinal modes $u_p(y)$ and $u_{p+1}(y)$ are active at the same time, they produce vibrations of the carrier densities $\delta n(y)$ and the distribution functions $\delta f_k(y)$ which in turn change the optical gain $g(y)$. Contributions to $\delta n(y)$ and $\delta f_k(y)$ with a strong spatial dependence are quickly damped due to carrier diffusion, therefore only the contributions with a weak spatial dependence need to be considered. In the derivation, the equations of motion for the charge carriers are solved approximately and the resulting deviations δf_k are substituted into the equations of motion for the photon numbers in order to obtain an effective mode interaction term.

where λ_p represents the vacuum wavelength of mode p , c is the speed of light in vacuum, τ_{in} is denoted as the intraband relaxation time, and B is the self-saturation coefficient which depends on various other parameters. For a large mode spacing, the antisymmetric mode interaction matrix H_{pq} can be expressed as:

$$H_{pq} = \frac{3\lambda_p^2}{8\pi c} \left(\frac{a\xi}{V} \right)^2 \frac{\alpha(N - N_g)}{\lambda_q - \lambda_p}. \quad (10)$$

Here, a denotes the slope coefficient to determine the local linear gain, N_g represents the transparent electron number, V is the volume of the active region, ξ is the confinement factor, and α denotes the linewidth enhancement factor. It is worth noting that in this model, the scattering and dephasing effects are incorporated into a single parameter τ_{in} , which corresponds to the scattering time τ_s in Eq. (8). In the subsequent section, we derive a mode interaction term that allows for a more detailed description of the scattering processes.

2.3 Derivation of the mode interaction terms

The mode interaction term derived in this section has the form

$$\left. \frac{d}{dt} S_p \right|_{\text{Interaction}} \approx \sum_q \frac{S_p S_q}{\omega_p \omega_q} \int d^2 \mathbf{r}_{\parallel} |\mathbf{u}_p(\mathbf{r}_{\parallel})|^2 |\mathbf{u}_q(\mathbf{r}_{\parallel})|^2 G(\omega_q - \omega_p, \mathbf{r}_{\parallel}). \quad (11)$$

This expression can be easily incorporated into rate equations for the photon numbers S_p as an additional term and can also be used for multiple lateral modes. In the case of multiple quantum wells the same formula can be used, the integral just needs to be evaluated for every quantum well.

Thus, the strength of the mode interaction between two modes p and q is determined by a function $G(\Delta\omega, \mathbf{r}_{\parallel})$ that depends on the frequency difference $\Delta\omega = \omega_q - \omega_p$, the temperature and the carrier

densities at the point \mathbf{r}_{\parallel} . In the following we present a microscopic derivation of the mode interaction strength $G(\Delta\omega, \mathbf{r}_{\parallel})$.

In a laser diode, the photon numbers and distribution functions generally exhibit a relatively slow change over a time scale of nanoseconds, particularly once the turn-on process is complete. However, the dephasing times for semiconductors are on the order of 100 fs [39], therefore Eq. (2) can be approximately solved for the polarization:

$$\begin{aligned}\psi_{\mathbf{k}}^{\lambda} &= \sum_p \frac{ep_{\lambda}^*}{m_0} \sqrt{\frac{\hbar}{2\omega_p\epsilon_0}} u_p(\mathbf{r}_{\parallel}) B_p \sum_{\mathbf{k}'} \Lambda_{\mathbf{k}\mathbf{k}'}^{\lambda,-1}(\omega_p) (1 - f_{\mathbf{k}'}^e - f_{\mathbf{k}'}^{\lambda}) \\ &= - \sum_p \frac{ep_{\lambda}^*}{m_0} \sqrt{\frac{\hbar}{2\omega_p\epsilon_0}} u_p(\mathbf{r}_{\parallel}) B_p \chi_{\mathbf{k}}^{\lambda}(\omega_p),\end{aligned}\quad (12)$$

where $\Lambda_{\mathbf{k}\mathbf{k}'}^{\lambda,-1}$ denotes the inverse of the matrix

$$\Lambda_{\mathbf{k}\mathbf{k}'}^{\lambda}(\omega) = \delta_{\mathbf{k}\mathbf{k}'} (\hbar\omega - \tilde{\epsilon}_{\mathbf{k}}^e - \tilde{\epsilon}_{\mathbf{k}}^{\lambda}) + i\Gamma_{\mathbf{k}\mathbf{k}'}^{\lambda} + \frac{1}{A} (1 - f_{\mathbf{k}}^e - f_{\mathbf{k}}^{\lambda}) V_{\mathbf{k}'-\mathbf{k}}^{\text{e}\lambda}.$$

Here $\chi_{\mathbf{k}}^{\lambda}(\omega)$ denotes contributions for wavevector \mathbf{k} and hole band λ to the electrical susceptibility

$$\chi(\omega) = \frac{2}{A} \sum_{\lambda\mathbf{k}} \frac{e^2 |p_{\lambda}|^2}{\epsilon_0 m_0^2 \omega^2} \chi_{\mathbf{k}}^{\lambda}(\omega). \quad (13)$$

While the real part of the susceptibility determines changes in the refractive index, the imaginary part of the susceptibility is strongly related to the absorption and therefore the optical gain [40]

$$g(\omega) = -\frac{\omega}{n(\omega)cd_{\text{QW}}} \text{Im} \chi(\omega),$$

where $n(\omega)$ is the refractive index, c is the speed of light in vacuum and d_{QW} is the quantum well thickness. The equations of motion for the photon numbers can be obtained by substituting Eqs. (4) and (12) into Eq. (1):

$$\frac{d}{dt} S_p = \sum_q \text{Im} \left\{ B_p^* B_q \frac{C_{\lambda}}{\sqrt{\omega_p \omega_q}} \int d^2\mathbf{r}_{\parallel} u_p^*(\mathbf{r}_{\parallel}) u_q(\mathbf{r}_{\parallel}) \frac{2}{A} \sum_{\lambda\mathbf{k}} \chi_{\mathbf{k}}^{\lambda}(\omega_q) \right\}, \quad (14)$$

with the abbreviation $C_{\lambda} = e^2 |p_{\lambda}|^2 / m_0^2 \epsilon_0$. The initial step involves isolating the highly time-dependent contributions of the distribution functions that are induced by two distinct active optical modes, distinguishing them from the remaining terms:

$$f_{\mathbf{k}}(\mathbf{r}_{\parallel}) = f_{\mathbf{k}}^0(\mathbf{r}_{\parallel}) + \delta f_{\mathbf{k}}(\mathbf{r}_{\parallel}).$$

Here the contributions with a strong time dependence are given by $\delta f_{\mathbf{k}}(\mathbf{r}_{\parallel})$. For example, the frequency difference of two neighbouring longitudinal modes is given approximately by 0.5 ps^{-1} for the structure discussed in section 3, where as the term $f_{\mathbf{k}}^0(\mathbf{r}_{\parallel})$ is assumed to change on a nanosecond timescale. For the current discussion we assume that the distribution functions $f_{\mathbf{k}}^0$ are given by Fermi-Dirac distributions. Substituting the solution from Eq. (12) for the microscopic polarization into the equations of motion for the distribution functions in Eqs. (6) yields

$$\begin{aligned}\frac{d}{dt} f_{\mathbf{k}}^e &= \sum_{\lambda} \sum_{pq} C_{\lambda} \frac{1}{\sqrt{\omega_q \omega_p}} \text{Im} \{ B_p B_q^* \chi_{\mathbf{k}}^{\lambda}(\omega_p) u_p(\mathbf{r}_{\parallel}) u_q^*(\mathbf{r}_{\parallel}) \} - \frac{f_{\mathbf{k}}^e}{\tau_{\text{nr}}} - \sum_{\mathbf{k}'} J_{\mathbf{k}\mathbf{k}'}^e (f_{\mathbf{k}'}^e - f_{\mathbf{k}'}^{\text{e,FD}}), \\ \frac{d}{dt} f_{\mathbf{k}}^{\lambda} &= \sum_{pq} C_{\lambda} \frac{1}{\sqrt{\omega_q \omega_p}} \text{Im} \{ B_p B_q^* \chi_{\mathbf{k}}^{\lambda}(\omega_p) u_p(\mathbf{r}_{\parallel}) u_q^*(\mathbf{r}_{\parallel}) \} - \frac{f_{\mathbf{k}}^{\lambda}}{\tau_{\text{nr}}} - \sum_{\mathbf{k}'} J_{\mathbf{k}\mathbf{k}'}^{\lambda} (f_{\mathbf{k}'}^{\lambda} - f_{\mathbf{k}'}^{\lambda,\text{FD}}).\end{aligned}\quad (15)$$

The equation of motion for the spatial deviations of the hole distribution functions is then given by

$$\begin{aligned} \frac{d}{dt} \delta f_{\mathbf{k}}^{\lambda} \approx & \sum_{p \neq q} C_{\lambda} \frac{1}{\sqrt{\omega_q \omega_p}} \text{Im} \left\{ B_p B_q^* \chi_{\mathbf{k}}^{\lambda}(\omega_p) u_p(\mathbf{r}_{\parallel}) u_q^*(\mathbf{r}_{\parallel}) \right\} \\ & - \sum_{\mathbf{k}'} J_{\mathbf{k}\mathbf{k}'}^{\lambda} \left(\delta f_{\mathbf{k}'}^{\lambda} - \delta n_h \frac{\partial f_{\mathbf{k}'}^{\lambda, \text{FD}}}{\partial n_h^0} \right) - \frac{\delta f_{\mathbf{k}}^{\lambda}}{\tau_{\text{nr}}}, \end{aligned}$$

where $\frac{\partial f_{\mathbf{k}'}^{\lambda, \text{FD}}}{\partial n_h^0}$ denotes the derivative of the Fermi-Dirac distributions with respect to the density and

$$\delta n_h = \frac{2}{A} \sum_{\lambda \mathbf{k}} \delta f_{\mathbf{k}}^{\lambda}$$

is the deviation of the hole density. An analogous equation of motion can be derived for the electrons. When the densities and photon numbers change slowly compared to the typical scattering times, it is possible to solve these equations of motion approximately and we obtain for the spatial deviations of the hole distribution functions:

$$\begin{aligned} \delta f_{\mathbf{k}}^{\lambda} \approx & \sum_{\lambda' p q, p > q} C_{\lambda'} \sqrt{\frac{1}{\omega_q \omega_p}} \text{Re} \left\{ B_p B_q^* u_p(\mathbf{r}_{\parallel}) u_q^*(\mathbf{r}_{\parallel}) \right. \\ & \times \left(\delta_{\lambda \lambda'} \sum_{\mathbf{k}'} \tilde{J}_{\mathbf{k}\mathbf{k}'}^{\lambda}(\omega_q - \omega_p) (\text{Im} \chi_{\mathbf{k}'}^{\lambda, 0}(\omega_p) + \text{Im} \chi_{\mathbf{k}'}^{\lambda, 0}(\omega_q)) \right. \\ & \left. \left. - \frac{i}{\omega_q - \omega_p} (\text{Im} \chi_{\lambda'}^0(\omega_p) + \text{Im} \chi_{\lambda'}^0(\omega_q)) \sum_{\mathbf{k}''} \tilde{J}_{\mathbf{k}\mathbf{k}'}^{\lambda, -1}(\omega_q - \omega_p) J_{\mathbf{k}'\mathbf{k}''}^{\lambda} \frac{\partial f_{\mathbf{k}''}^{\lambda, \text{FD}}}{\partial n_h^0} \right) \right\}. \quad (16) \end{aligned}$$

A similar expression can be derived for the electron distribution functions. Here χ_{λ} denotes the contribution of the valence band with index λ to the susceptibility in Eq. (13):

$$\chi_{\lambda}(\omega) = \frac{2}{A} \sum_{\mathbf{k}} \chi_{\mathbf{k}}^{\lambda}(\omega).$$

The corrected scattering matrix $\tilde{J}_{\mathbf{k}\mathbf{k}'}^{\lambda}$ is defined as

$$\tilde{J}_{\mathbf{k}\mathbf{k}'}^{\lambda}(\Delta\omega) = J_{\mathbf{k}\mathbf{k}'}^{\lambda} + i\Delta\omega \delta_{\mathbf{k}\mathbf{k}'} - C_{\lambda} \sum_p \frac{S_p}{\omega_p} |u_p(\mathbf{r}_{\parallel})|^2 \text{Im} \Lambda_{\mathbf{k}\mathbf{k}'}^{\lambda, -1}(\omega_p). \quad (17)$$

In the case of a vanishing frequency difference ($\Delta\omega \rightarrow 0$) and no photons ($S_p = 0$) the corrected scattering matrix is given by the scattering matrix in Eq. (7). The approximation from Eq. (16) can be inserted into the equation of motion of the photon numbers (14) to obtain an effective mode interaction

term:

$$\begin{aligned}
\left. \frac{d}{dt} S_p \right|_{\text{Interaction}} &= \\
&- \sum_{\substack{\lambda\lambda'qrs \\ r>s, q\neq p}} \frac{C_\lambda C_{\lambda'}}{\sqrt{\omega_p \omega_q \omega_r \omega_s}} \text{Im} \left\{ B_p^* B_q \int d^2 \mathbf{r}_{\parallel} u_p^*(\mathbf{r}_{\parallel}) u_q(\mathbf{r}_{\parallel}) \frac{2}{A} \sum_{\mathbf{k}\mathbf{k}'} \Lambda_{\mathbf{k}\mathbf{k}'}^{\lambda, -1}(\omega_q) \right. \\
&\times \text{Re} \left\{ B_r B_s^* u_r(\mathbf{r}_{\parallel}) u_s^*(\mathbf{r}_{\parallel}) \right. \\
&\quad \times \left(\sum_{\mathbf{k}''} [\tilde{J}_{\mathbf{k}'\mathbf{k}''}^{e, -1}(\omega_s - \omega_r) + \delta_{\lambda\lambda'} \tilde{J}_{\mathbf{k}'\mathbf{k}''}^{\lambda, -1}(\omega_s - \omega_r)] \left(\text{Im} \chi_{\mathbf{k}''}^{\lambda', 0}(\omega_r) + \text{Im} \chi_{\mathbf{k}''}^{\lambda', 0}(\omega_s) \right) \right. \\
&\quad \left. \left. - i \frac{\text{Im} \chi_{\lambda'}^0(\omega_r) + \text{Im} \chi_{\lambda'}^0(\omega_s)}{\omega_s - \omega_r} \right. \right. \\
&\quad \left. \left. \times \sum_{\mathbf{k}''\mathbf{k}'''} \left[\tilde{J}_{\mathbf{k}'\mathbf{k}''}^{e, -1}(\omega_s - \omega_r) J_{\mathbf{k}''\mathbf{k}'''}^e \frac{\partial f_{\mathbf{k}'''}^{e, \text{FD}}}{\partial n_e^0} + \tilde{J}_{\mathbf{k}'\mathbf{k}''}^{\lambda, -1}(\omega_s - \omega_r) J_{\mathbf{k}''\mathbf{k}'''}^\lambda \frac{\partial f_{\mathbf{k}'''}^{\lambda, \text{FD}}}{\partial n_h^0} \right] \right) \right\}.
\end{aligned}$$

This effective interaction is initially rather complicated and can be simplified further by assuming that only the dominant contributions with $r = p, s = q$ or $r = q, s = p$ contribute. In comparison, the other contributions oscillate with the frequency differences of the form $\omega_p - \omega_q$ and are almost negligible when averaged over time, see also Ref. [20]. We also assume that all relevant modes are close to the gain maximum in terms of frequency. This can be used to approximately replace all the frequencies with the frequency ω_0 of the gain maximum, except in places where the frequency difference $\omega_p - \omega_q$ is calculated. This results in a mode interaction term as in Eq. (11), where the strength of the interaction only depends on the frequency difference of the modes and the state of the carriers in the quantum well, and is given by

$$\boxed{
\begin{aligned}
G(\Delta\omega) &= - \sum_{\lambda\lambda'} C_\lambda C_{\lambda'} \text{Im} \left\{ \frac{2}{A} \sum_{\mathbf{k}\mathbf{k}'} \Lambda_{\mathbf{k}\mathbf{k}'}^{\lambda, -1}(\omega_0) \left(\sum_{\mathbf{k}''} [\tilde{J}_{\mathbf{k}'\mathbf{k}''}^{e, -1}(\Delta\omega) + \delta_{\lambda\lambda'} \tilde{J}_{\mathbf{k}'\mathbf{k}''}^{\lambda, -1}(\Delta\omega)] \text{Im} \chi_{\mathbf{k}''}^{\lambda', 0}(\omega_0) \right. \right. \\
&\quad \left. \left. - i \frac{\text{Im} \chi_{\lambda'}^0(\omega_0)}{\Delta\omega} \sum_{\mathbf{k}''\mathbf{k}'''} \left[\tilde{J}_{\mathbf{k}'\mathbf{k}''}^{e, -1}(\Delta\omega) J_{\mathbf{k}''\mathbf{k}'''}^e \frac{\partial f_{\mathbf{k}'''}^{e, \text{FD}}}{\partial n_e^0} + \tilde{J}_{\mathbf{k}'\mathbf{k}''}^{\lambda, -1}(\Delta\omega) J_{\mathbf{k}''\mathbf{k}'''}^\lambda \frac{\partial f_{\mathbf{k}'''}^{\lambda, \text{FD}}}{\partial n_h^0} \right] \right) \right\}.
\end{aligned}
} \tag{18}$$

The matrix $\tilde{J}_{\mathbf{k}\mathbf{k}'}^\lambda$ is now determined by

$$\tilde{J}_{\mathbf{k}\mathbf{k}'}^\lambda(\Delta\omega) = J_{\mathbf{k}\mathbf{k}'}^\lambda + i\Delta\omega \delta_{\mathbf{k}\mathbf{k}'} - C_\lambda \frac{s}{\omega_p} \text{Im} \Lambda_{\mathbf{k}\mathbf{k}'}^{\lambda, -1}(\omega_0), \tag{19}$$

with the photon density $s = \sum_p S_p |u_p(\mathbf{r}_{\parallel})|^2$. Like any other function, the mode interaction can be separated into symmetric and antisymmetric contributions with respect to the frequency difference $\Delta\omega$:

$$G(\Delta\omega) = G_S(\Delta\omega) + G_A(\Delta\omega).$$

2.4 Analysis for a constant scattering time

For a general scattering matrix the mode interaction term in equation (18) needs to be evaluated numerically. However, for the special case of a constant scattering time τ_s the mode interaction can be

simplified. In this case the scattering matrix is given by

$$J_{\mathbf{k}\mathbf{k}'}^\lambda = \frac{1}{\tau_s} \delta_{\mathbf{k}\mathbf{k}'}$$

As a scattering term of this form was used by Yamada et al. the resulting mode interaction terms should agree with equations (9) and (10). In the limit of a small scattering time $\tau_s \ll 1/\Delta\omega$ and a vanishing photon density $s = 0$ we obtain the symmetric interaction term

$$G_S(\Delta\omega) = \frac{G(\Delta\omega) + G(-\Delta\omega)}{2} = - \sum_{\lambda\lambda'} C_\lambda C_{\lambda'} \frac{\tau_s(1 + \delta_{\lambda\lambda'})}{\Delta\omega^2 \tau_s^2 + 1} \frac{2}{A} \sum_{\mathbf{k}\mathbf{k}'} \text{Im} \Lambda_{\mathbf{k}\mathbf{k}'}^{\lambda,-1}(\omega_0) \text{Im} \chi_{\mathbf{k}'}^{\lambda',0}(\omega_0) + \omega_0^4 \text{Im} \chi(\omega_0) \text{Im} \chi'(\omega_0) \frac{\tau_s}{\Delta\omega^2 \tau_s^2 + 1} \quad (20)$$

and the antisymmetric interaction term

$$G_A(\Delta\omega) = \frac{G(\Delta\omega) - G(-\Delta\omega)}{2} = \omega_0^4 \frac{\text{Im} \chi(\omega_0) \text{Re} \chi'(\omega_0)}{\Delta\omega}. \quad (21)$$

Here $\chi'(\omega)$ denotes the derivative of the susceptibility with respect to the carrier densities:

$$\chi'(\omega) = \frac{\partial \chi(\omega)}{\partial n_e} + \frac{\partial \chi(\omega)}{\partial n_h}.$$

In order to see how Eq. (21) relates to Eq. (10) from Yamada et al., we can use the antiguiding factor or linewidth-enhancement factor α to express the derivative of the real part of the susceptibility in terms of the derivative of the imaginary part [39]:

$$\alpha = \frac{\text{Re} \chi'(\omega)}{\text{Im} \chi'(\omega)}.$$

Under the assumption of linear gain

$$\text{Im} \chi(\omega) \propto \frac{\xi a}{V} (N - N_g) \Rightarrow \text{Im} \chi'(\omega) \propto \frac{\xi a}{V}$$

and replacing the frequency difference $\Delta\omega \approx -2\pi c \Delta\lambda / \lambda_0^2$, Eq. (21) becomes

$$G_A(\Delta\lambda) \propto \left(\frac{\xi a}{V} \right)^2 \frac{\alpha (N - N_g)}{\Delta\lambda}.$$

The remaining prefactor in Eq. (11) can be determined by evaluating the integral using a lateral mode of the form $\sin(\pi x/w_r)$, where w_r represents the ridge width, and assuming constant carrier densities. The only difference is an additional factor of 2, which can be attributed to carrier diffusion and will be discussed in the subsequent section. In equations (9) and (20), the symmetric mode interaction term exhibits a frequency dependence of $((\Delta\omega\tau_s)^2 + 1)^{-1}$ in both cases.

2.5 Influence of carrier diffusion

One aspect that is yet to be considered is the diffusion of carriers in the quantum well, which can dampen the beating vibrations of the carrier densities and therefore reduce the mode interaction. If

we consider as an example longitudinal modes described by standing waves ($u_p(y) \propto \sin(p\pi y/L)$), then the beating vibrations will be of the form

$$\frac{d}{dt} \delta n(y) \propto u_p(y) u_q(y) \propto \sin\left(\frac{p\pi y}{L}\right) \sin\left(\frac{q\pi y}{L}\right) \propto \cos\left(\frac{(p-q)\pi y}{L}\right) - \cos\left(\frac{(p+q)\pi y}{L}\right) \quad (22)$$

For a green nitride laser diode we might have a resonator length $L = 600 \mu\text{m}$, a refractive index of 2.4 and a laser wavelength of 500 nm, which results in $p \approx q \approx 5760$. Using the diffusion equation and a diffusion constant of $10 \text{ cm}^2 \text{ s}^{-1}$ the second term in Eq. (22) is dampened with a time constant of $\tau \approx 0.3 \text{ ps}$ and therefore should not contribute to the mode dynamics. For two neighbouring modes ($q = p + 1$) the time constant for the first term is given by $\tau \approx 37 \text{ fs}$ and the dampening due to diffusion can be neglected. As both terms in Eq. (22) contribute equally to the mode interaction in Eq. (11) we can include the effect of carrier diffusion using an additional factor of $1/2$:

$$\left. \frac{d}{dt} S_p \right|_{\text{Interaction}} \approx \frac{1}{2} \sum_q \frac{S_p S_q}{\omega_p \omega_q} \int d^2 \mathbf{r}_{\parallel} |u_p(\mathbf{r}_{\parallel})|^2 |u_q(\mathbf{r}_{\parallel})|^2 G(\omega_q - \omega_p, \mathbf{r}_{\parallel}). \quad (23)$$

3 Results

To compute the mode interaction terms, it is necessary to have knowledge of the quantum well's band structure, optical matrix elements, and Coulomb matrix elements. To achieve this, the $\mathbf{k} \cdot \mathbf{p}$ method is employed for an InGaN quantum well encapsulated by GaN, utilizing the Hamiltonian proposed by Chuang et al. [41]. The equations that were used in the calculations can be found in the appendix and the parameters are provided in Ref. [42]. The quantum well is composed of 28% indium, and it has a thickness of 2 nm. The refractive index of GaN is known to be 2.4 for wavelengths near 550 nm [42]. The Coulomb interaction uses the static dielectric constant of the surrounding GaN material, with a value of 9.7 [43]. During the numerical computation of the scattering terms, the delta functions are substituted with Lorentzian functions with a broadening of 5 meV. Additionally, the broadening in the Lindhard formula [39, 44] is set to 10 meV. In the calculations the Piezo effect is included [42, 45] with a fixed carrier density of 10^{13} cm^{-2} in the quantum well and a temperature of 300 K. In the solution of the Poisson equation a vanishing electrical field at the boundaries of the simulation cell is assumed. In the following calculation of the mode interaction terms, different scattering terms are used, but the dephasing of the microscopic polarization is always determined by Coulomb scattering with dynamic screening. The resulting susceptibility is shown in Fig. 2.

In Fig. 3 a) and c) a microscopic analysis of the symmetric and antisymmetric mode interaction terms is shown using a constant scattering time for different carrier densities. The interaction term is evaluated at the gain maximum, therefore only carrier densities above transparency are used in the calculations. The photon density in Eq. (17) is set to zero, as it has a small effect on the mode interaction for a constant scattering time (see the appendix). For the largest carrier density the approximations of Eq. (20) and Eq. (21) are also shown and agree reasonably with the calculation using Eq. (18). While the antisymmetric contribution diverges as the frequency difference goes to zero, the symmetric contribution has the form of a Lorentzian function, where the broadening is determined by the scattering time. A larger carrier density leads to a stronger mode interaction, especially for the symmetric contribution.

In Fig. 3 b) and d) Coulomb scattering was used to calculate the mode interaction terms for different carrier densities and a vanishing photon density. The antisymmetric term shows a behavior similar to the calculation with the constant scattering time, but does not quite agree with the approximation of

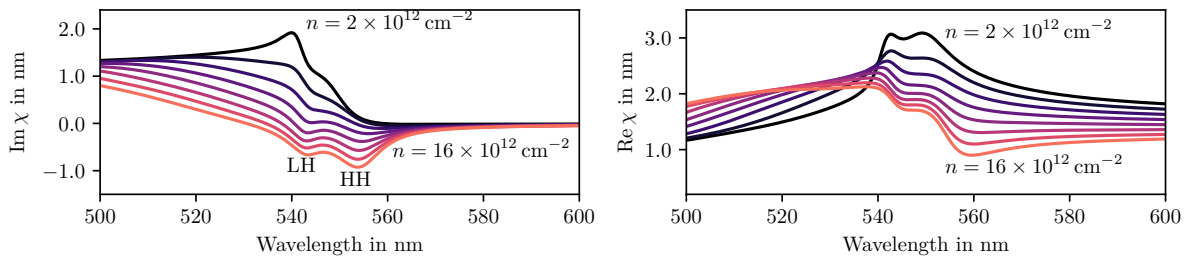


Figure 2: Electronic susceptibility from Eq. (13) calculated using the $\mathbf{k} \cdot \mathbf{p}$ bandstructure and Coulomb scattering. The carrier density was systematically varied from $2 \times 10^{12} \text{ cm}^{-2}$ to $16 \times 10^{12} \text{ cm}^{-2}$ in increments of $2 \times 10^{12} \text{ cm}^{-2}$. Due to the large energy difference between the second and the third hole band in the $\mathbf{k} \cdot \mathbf{p}$ calculations, only the first two hole bands are considered in the simulations. This results in two peaks in the imaginary part of the susceptibility, which is nearly proportional to the absorption spectrum. The lower wavelength peak belongs to transitions between the conduction band and the first light hole band (LH) and the higher wavelength peak is due to transitions between the conduction band and the first heavy hole band (HH).

Eq. (21). More interestingly, the symmetric term shows a very different behavior in comparison and diverges for $\Delta\omega \rightarrow 0$. In both cases the interaction strength increases for higher carrier densities.

The effect of the photon density in Eq. (19) is investigated in Fig. 4 for a constant scattering time and Coulomb scattering. For a constant scattering time the photon density only causes a small reduction of the mode interaction strength and has no influence on the qualitative behavior. For nonzero photon densities and Coulomb scattering the symmetric term no longer diverges for $\Delta\omega \rightarrow 0$ and shows a similar behavior compared to the calculation with a constant scattering time. While a higher photon density decreases the strength of the mode interaction for small frequency differences, there is an increase in the interaction for large $\Delta\omega$. Interestingly enough the divergence of the antisymmetric interaction is also lifted for nonzero photon densities while the behavior for larger frequency differences remains unaffected.

An example for the mode dynamics of a Fabry-Pérot laser diode using these effective mode interaction terms is shown in Fig. 5 for different current densities. For these calculations the equations of motion from Ref. [9] are used, with the difference that all the third order effects are replaced by the effective mode interaction terms. The resulting set of equations is also shown in the appendix. For this example a resonator length of $600 \mu\text{m}$, a ridge width of $2 \mu\text{m}$, an injection efficiency of 0.75, a group refractive index of 2.8, a photon lifetime of 16 ps and a nonradiative recombination time of 1000 ns are used. The broadening of the gain spectrum due to Coulomb scattering is not sufficient to obtain realistic results, therefore an additional inhomogeneous broadening of 30 meV is included in the calculation. In both cases the effect of mode hopping can be seen, where the currently active mode changes from smaller to higher wavelengths, which can be observed experimentally [8, 20]. Once the gain for the active mode is not sufficient anymore this process restarts at the gain maximum. The mode rolling frequency is determined by the period of this process and increases with increasing current densities. For a scattering time of 100 fs the mode rolling frequencies are too large compared to the calculation with Coulomb scattering, therefore the scattering time is increased to 300 fs in Fig. 5 in order to produce very similar mode rolling frequencies. In this case the resulting mode dynamics are comparable and only show major differences at the beginning of the simulations. Here the calculation using Coulomb scattering shows a better qualitative behavior compared to experimental results [8, 20].

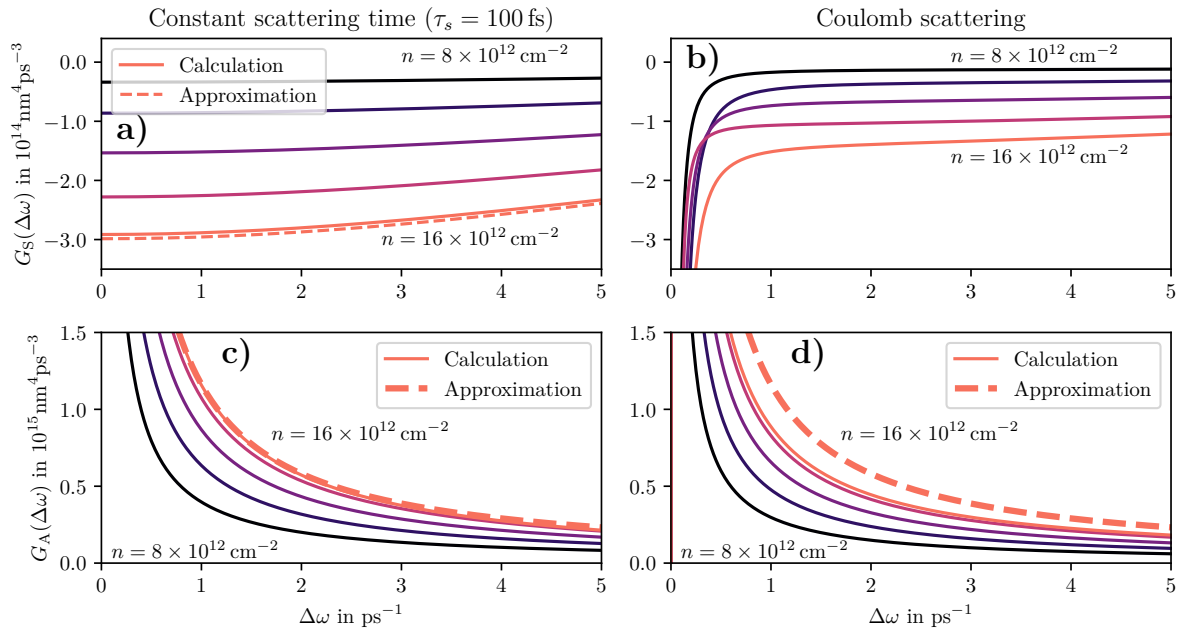


Figure 3: Mode interaction of Eq. (18) as a function of the frequency difference of the two modes. In the two figures on the left a constant scattering time $\tau_s = 100$ fs was used, and Coulomb scattering in the two figures on the right. The symmetric contributions to the mode interaction are shown in a) and b) where as the antisymmetric contributions are shown in c) and d). The mode interaction is depicted for various carrier densities, ranging from $8 \times 10^{12} \text{ cm}^{-2}$ to $16 \times 10^{12} \text{ cm}^{-2}$, with increments of $2 \times 10^{12} \text{ cm}^{-2}$. The calculations were performed with zero photon density. For comparison the approximations from Eq. (20) and Eq. (21) are also shown for the highest carrier density.

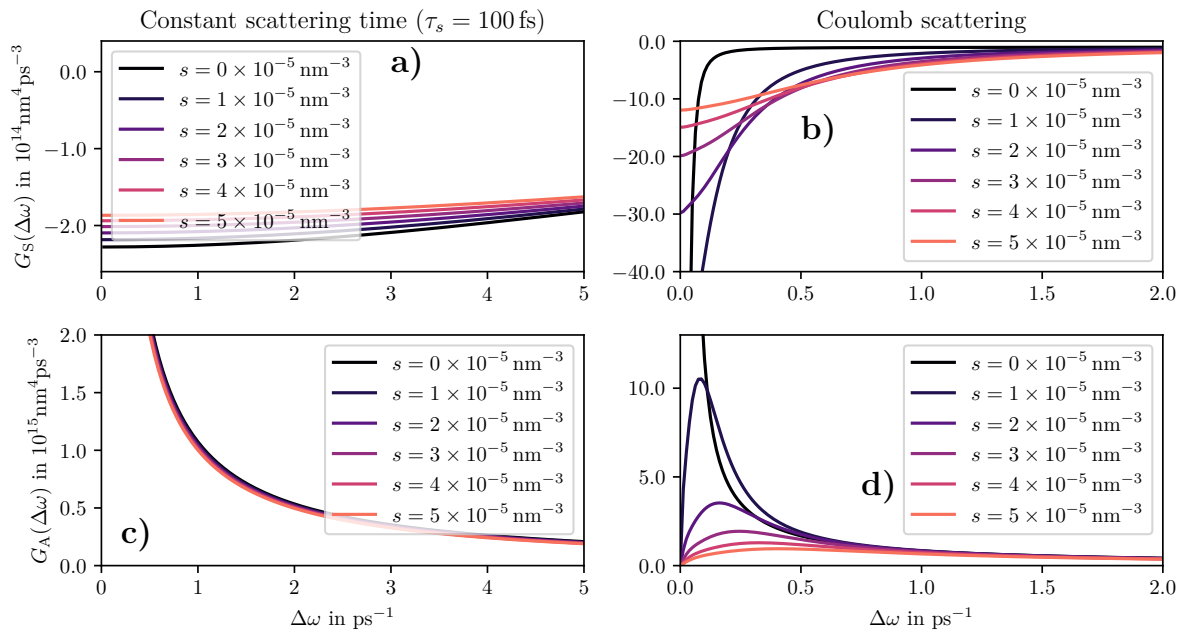


Figure 4: Mode interaction of Eq. (18) for Coulomb scattering as a function of the frequency difference for a fixed carrier density of $1.4 \times 10^{13} \text{ cm}^{-2}$ and different photon densities. In the two figures on the left a constant scattering time $\tau_s = 100$ fs was used, and Coulomb scattering in the two figures on the right.

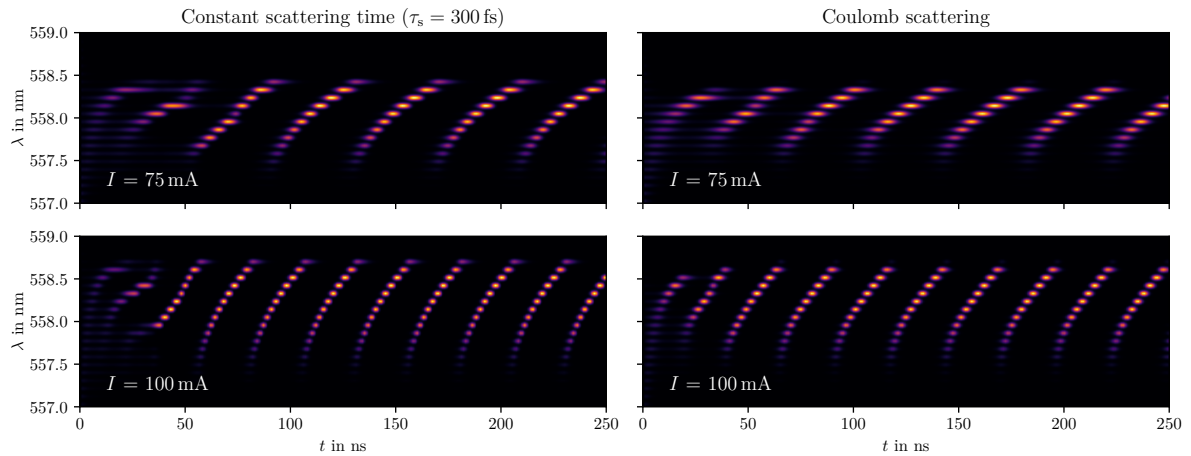


Figure 5: The longitudinal mode dynamics of a Fabry-Pérot laser diode for two different currents. Here the output of the laser is shown as a function of wavelength and time. The data for this figure is calculated by multiplying the time-dependent photon numbers from the simulation with Gaussian functions that are centered at their respective vacuum wavelengths with a width of 0.02 nm. On the left the mode interaction terms were calculated using a constant scattering time of 300 fs and on the right the Coulomb scattering term was used.

4 Summary

Fabry-Pérot type laser diodes show mode competition effects that can be simulated with rate equations using an effective mode interaction term. In this paper, a mode interaction term was derived that can be used for different scattering mechanisms and when more than one lateral mode is relevant. While the mode interaction terms have no impact on the output power of the laser diode, they determine the level of activity of individual modes. For a constant scattering time the results agree with mode interaction terms found in literature. In comparison, the mode interaction terms for Coulomb scattering show a very different behavior, especially for $\Delta\omega \rightarrow 0$, where $\Delta\omega$ is the frequency difference of the two interacting modes. While the form of the mode interaction terms is more complex, in typical simulations they can be calculated for different carrier densities before the actual mode dynamics simulation and thus have a negligible impact on the performance. While all the calculations in this paper have been performed using Coulomb scattering, it is possible to include other scattering mechanisms such as electron-phonon scattering. In this paper the influence of the photon density on the strength of mode interaction is also discussed. While a nonzero photon density has a small effect on the mode interaction for a constant scattering time, for Coulomb scattering qualitative changes can be observed. For example the mode interaction term no longer diverges for $\Delta\omega \rightarrow 0$ for nonzero photon densities. Therefore the dependence of the mode interaction on the field intensity should be considered in rate equation simulations, when a realistic scattering term is used. The effect of the scattering terms on the mode dynamics using an effective mode interaction term was also studied for a simple example where the carrier densities were assumed to be constant in the quantum well. If the scattering time is chosen appropriately the mode dynamics are very similar, but using Coulomb scattering results in a more realistic behavior at the beginning of the simulation. In conclusion, the mode interaction terms derived in this paper offer a way to simulate the mode dynamics in different kinds of laser diodes. They are especially important for laser diodes with a small mode spacing, for example Fabry-Pérot

laser diodes with broad and narrow ridge widths. Compared to using a constant scattering time, more complex scattering times offer an increased predictability due to better known parameters and also improve the behavior of the mode dynamics at the beginning of the simulation.

Acknowledgements

This work was performed in the frame of the German Leibniz Association funded project PCSElence (K487/2022).

References

- [1] L. Jiang *et al.*, “GaN-based green laser diodes”, *Journal of Semiconductors*, vol. 37, no. 11, p. 111 001, Nov. 2016. DOI: 10.1088/1674-4926/37/11/111001.
- [2] Y. Nakatsu *et al.*, “High-efficiency blue and green laser diodes for laser displays”, *Proc. SPIE*, vol. 10918, 2019. DOI: 10.1117/12.2505309.
- [3] N. Shimada, M. Yukawa, K. Shibata, K. Ono, T. Yagi, and A. Shima, “640-nm laser diode for small laser display”, *Proc. SPIE*, vol. 7198, 2009. DOI: 10.1117/12.808710.
- [4] S. Masui, T. Miyoshi, T. Yanamoto, and S.-I. Nagahama, “Blue and green laser diodes for large laser display”, *Proc. CLEOPR*, 2013. DOI: 10.1109/CLEOPR.2013.6599913.
- [5] D. Queren *et al.*, “500 nm electrically driven ingan based laser diodes”, *Applied Physics Letters*, vol. 94, no. 8, p. 081 119, 2009. DOI: 10.1063/1.3089573.
- [6] S. Lutgen *et al.*, “Recent results of blue and green InGaN laser diodes for laser projection”, *Proc. SPIE*, vol. 7953, 2011. DOI: 10.1117/12.874757.
- [7] J. Raring *et al.*, “47.1: Invited paper: Progress in green and blue laser diodes and their application in pico projection systems”, *Digest of Technical Papers - SID International Symposium*, vol. 42 1, pp. 677–680, 2011. DOI: 10.1889/1.3621414.
- [8] T. Weig, T. Hager, G. Brüderl, U. Strauss, and U. T. Schwarz, “Longitudinal mode competition and mode clustering in (Al,In)GaN laser diodes”, *Optics Express*, vol. 22, no. 22, p. 27 489, Oct. 2014. DOI: 10.1364/oe.22.027489.
- [9] E. Kuhn, L. Uhlig, M. Wachs, U. Schwarz, and A. Thränhardt, “Mode rolling effects in nitride laser diodes”, *Engineering Research Express*, vol. 2, no. 3, 2020. DOI: 10.1088/2631-8695/abb6c8.
- [10] L. Uhlig, D. J. Kunzmann, and U. T. Schwarz, “Characterization of lateral and longitudinal mode competition in blue ingan broad-ridge laser diodes”, *physica status solidi (a)*, vol. n/a, p. 2200751, 2022. DOI: <https://doi.org/10.1002/pssa.202200751>.
- [11] M. Yamada, “Theoretical analysis of nonlinear optical phenomena taking into account the beating vibration of the electron density in semiconductor lasers”, *Journal of Applied Physics*, vol. 66, no. 1, pp. 81–89, Jul. 1989. DOI: 10.1063/1.343860.
- [12] G. Agrawal and N. Olsson, “Self-phase modulation and spectral broadening of optical pulses in semiconductor laser amplifiers”, *IEEE Journal of Quantum Electronics*, vol. 25, no. 11, pp. 2297–2306, 1989. DOI: 10.1109/3.42059.
- [13] S. Balsamo, F. Sartori, and I. Montrosset, “Dynamic beam propagation method for flared semiconductor power amplifiers”, *IEEE Journal of Selected Topics in Quantum Electronics*, vol. 2, no. 2, pp. 378–384, 1996. DOI: 10.1109/2944.577398.
- [14] C. Ning, R. Indik, and J. Moloney, “Effective bloch equations for semiconductor lasers and amplifiers”, *IEEE Journal of Quantum Electronics*, vol. 33, no. 9, pp. 1543–1550, 1997. DOI: 10.1109/3.622635.
- [15] U. Bandelow, M. Radziunas, J. Sieber, and M. Wolfrum, “Impact of gain dispersion on the spatio-temporal dynamics of multisection lasers”, *IEEE Journal of Quantum Electronics*, vol. 37, no. 2, pp. 183–188, 2001. DOI: 10.1109/3.903067.

- [16] R. Iegis and M. Radziunas, “Effective numerical integration of traveling wave model for edge-emitting broad-area semiconductor lasers and amplifiers”, *Mathematical Modelling And Analysis*, vol. 15, pp. 409–430, Nov. 2010. DOI: 10.3846/1392-6292.2010.15.409-430.
- [17] M. Radziunas, *Modeling and Simulations of Edge-Emitting Broad-Area Semiconductor Lasers and Amplifiers*. Cham: Springer International Publishing, 2016, pp. 269–276, ISBN: 978-3-319-32152-3. DOI: 10.1177/1094342016677086.
- [18] M. Radziunas, “Modeling and simulations of broad-area edge-emitting semiconductor devices”, *The International Journal of High Performance Computing Applications*, vol. 32, no. 4, pp. 512–522, 2018. DOI: 10.1177/1094342016677086.
- [19] O. Hess and T. Kuhn, “Maxwell-Bloch equations for spatially inhomogeneous semiconductor lasers. I. theoretical formulation”, *Physical Review A*, vol. 54, no. 4, pp. 3347–3359, Oct. 1996. DOI: 10.1103/physreva.54.3347.
- [20] E. Kuhn and A. Thränhardt, “Modeling mode competition in laser diodes”, *Optical and Quantum Electronics*, vol. 51, no. 6, 2019. DOI: 10.1007/s11082-019-1916-7.
- [21] T. Weig, H. Höck, K. Holc, K. Köhler, J. Wagner, and U. T. Schwarz, “Implementation and investigation of mode locking in gan-based laser diodes in external cavity configuration”, *physica status solidi (a)*, vol. 212, no. 5, pp. 986–991, 2015. DOI: 10.1002/pssa.201431682.
- [22] W. E. Lamb, “Theory of an optical maser”, *Phys. Rev.*, vol. 134, A1429–A1450, 6A Jun. 1964. DOI: 10.1103/PhysRev.134.A1429.
- [23] M. Yamada, “Transverse and longitudinal mode control in semiconductor injection lasers”, *IEEE Journal of Quantum Electronics*, vol. 19, no. 9, pp. 1365–1380, Sep. 1983. DOI: 10.1109/jqe.1983.1072059.
- [24] M. Yamada, “Theory of mode competition noise in semiconductor injection lasers”, *IEEE Journal of Quantum Electronics*, vol. 22, no. 7, pp. 1052–1059, Jul. 1986. DOI: 10.1109/jqe.1986.1073087.
- [25] M. Ahmed, M. Yamada, and M. Saito, “Numerical modeling of intensity and phase noise in semiconductor lasers”, *IEEE Journal of Quantum Electronics*, vol. 37, no. 12, pp. 1600–1610, 2001. DOI: 10.1109/3.970907.
- [26] M. Ahmed and M. Yamada, “Influence of instantaneous mode competition on the dynamics of semiconductor lasers”, *IEEE Journal of Quantum Electronics*, vol. 38, no. 6, pp. 682–693, Jun. 2002. DOI: 10.1109/jqe.2002.1005419.
- [27] M. Ahmed, “Theoretical modeling of intensity noise in ingan-semiconductor lasers”, *The Scientific World Journal*, vol. 2014, p. 475 423, Jul. 2014. DOI: 10.1155/2014/475423.
- [28] J. Hader *et al.*, “Quantitative prediction of semiconductor laser characteristics based on low intensity photoluminescence measurements”, *IEEE Photonics Technology Letters*, vol. 14, no. 6, pp. 762–764, 2002. DOI: 10.1109/LPT.2002.1003085.
- [29] J. Hader, J. V. Moloney, S. W. Koch, and W. W. Chow, “Microscopic modeling of gain and luminescence in semiconductors”, *IEEE Journal of Selected Topics in Quantum Electronics*, vol. 9, no. 3, pp. 688–697, May 2003, ISSN: 1077-260X. DOI: 10.1109/JSTQE.2003.818342.
- [30] J. Hader, J. Moloney, and S. Koch, “Microscopic evaluation of spontaneous emission- and auger-processes in semiconductor lasers”, *IEEE Journal of Quantum Electronics*, vol. 41, no. 10, pp. 1217–1226, Oct. 2005. DOI: 10.1109/jqe.2005.854127.

- [31] A. Thränhardt *et al.*, “Nonequilibrium gain in optically pumped gainnas laser structures”, *Applied Physics Letters*, vol. 85, no. 23, pp. 5526–5528, 2004. DOI: 10.1063/1.1831570.
- [32] A. Thränhardt, S. Koch, J. Hader, and J. Moloney, “Carrier dynamics in quantum well lasers”, *Optical and Quantum Electronics*, vol. 38, no. 4-6, pp. 361–368, 2006, Cited by: 3. DOI: 10.1007/s11082-006-0036-3.
- [33] H. Haug and S. Schmitt-Rink, “Electron theory of the optical properties of laser-excited semiconductors”, *Progress in Quantum Electronics*, vol. 9, no. 1, pp. 3–100, 1984, ISSN: 0079-6727. DOI: [https://doi.org/10.1016/0079-6727\(84\)90026-0](https://doi.org/10.1016/0079-6727(84)90026-0).
- [34] S. Schmitt-Rink, C. Ell, and H. Haug, “Many-body effects in the absorption, gain, and luminescence spectra of semiconductor quantum-well structures”, *Phys. Rev. B*, vol. 33, pp. 1183–1189, 2 Jan. 1986. DOI: 10.1103/PhysRevB.33.1183.
- [35] F. Jahnke *et al.*, “Excitonic nonlinearities of semiconductor microcavities in the nonperturbative regime”, *Phys. Rev. Lett.*, vol. 77, pp. 5257–5260, 26 Dec. 1996. DOI: 10.1103/PhysRevLett.77.5257.
- [36] J. Hader, J. V. Moloney, A. Thränhardt, and S. W. Koch, “Interband Transitions in InGaN Quantum Wells”, in *Nitride Semiconductor Devices: Principles and Simulation*. John Wiley & Sons, Ltd, 2007, ch. 7, pp. 145–167, ISBN: 9783527610723. DOI: <https://doi.org/10.1002/9783527610723.ch7>.
- [37] M. Kira and S. W. Koch, *Semiconductor Quantum Optics*. Cambridge University Press, 2011. DOI: 10.1017/CBO9781139016926.
- [38] M. Lindberg and S. W. Koch, “Effective bloch equations for semiconductors”, *Phys. Rev. B*, vol. 38, pp. 3342–3350, 5 Aug. 1988. DOI: 10.1103/PhysRevB.38.3342.
- [39] H. Haug and S. Koch, *Quantum Theory of the Optical and Electronic Properties of Semiconductors*. World Scientific, 2009, ISBN: 9789812838834.
- [40] M. Lorke, T. R. Nielsen, J. Seebeck, P. Gartner, and F. Jahnke, “Influence of carrier-carrier and carrier-phonon correlations on optical absorption and gain in quantum-dot systems”, *Physical Review B - Condensed Matter and Materials Physics*, vol. 73, no. 8, p. 085324, 2006. DOI: 10.1103/PhysRevB.73.085324.
- [41] S. L. Chuang and C. S. Chang, “A band-structure model of strained quantum-well wurtzite semiconductors”, *Semiconductor Science and Technology*, vol. 12, no. 3, pp. 252–263, Mar. 1997. DOI: 10.1088/0268-1242/12/3/004.
- [42] J. Piprek, *Nitride Semiconductor Devices: Principles and Simulation*. Wiley, 2007, ISBN: 9783527610716.
- [43] I. Vurgaftman and J. R. Meyer, “Electron bandstructure parameters”, in *Nitride Semiconductor Devices: Principles and Simulation*. John Wiley & Sons, Ltd, 2007, ch. 2, pp. 13–48, ISBN: 9783527610723. DOI: <https://doi.org/10.1002/9783527610723.ch2>.
- [44] G. Stefanucci and R. van Leeuwen, *Nonequilibrium Many-Body Theory of Quantum Systems: A Modern Introduction*. Cambridge University Press, 2013, ISBN: 9780521766173.
- [45] T. R. Nielsen, P. Gartner, M. Lorke, J. Seebeck, and F. Jahnke, “Coulomb scattering in nitride-based self-assembled quantum dot systems”, *Physical Review B - Condensed Matter and Materials Physics*, vol. 72, no. 23, p. 235311, 2005. DOI: 10.1103/PhysRevB.72.235311.
- [46] J. D. Jackson, *Klassische Elektrodynamik*. De Gruyter, 2013, ISBN: 9783110334470. DOI: doi: 10.1515/9783110334470.

- [47] W. Schäfer and M. Wegener, *Semiconductor Optics and Transport Phenomena* (Advanced Texts in Physics). Springer, 2002, ISBN: 9783540616146. DOI: 10.1007/978-3-662-04663-0.

A $\mathbf{k} \cdot \mathbf{p}$ Hamiltonian

For the calculation of the band structure of an InGaN quantum well, we employ the Hamiltonian proposed by Chuang et al. [41]. This Hamiltonian is expressed as follows:

$$\hat{H} = \begin{pmatrix} F & -H^* & -K^* & 0 & 0 & 0 \\ -H & \lambda & H^* & \Delta & 0 & 0 \\ -K & H & G & 0 & \Delta & 0 \\ 0 & \Delta & 0 & G & -H^* & -K^* \\ 0 & 0 & \Delta & -H & \lambda & H^* \\ 0 & 0 & 0 & -K & H & F \end{pmatrix} \quad (24)$$

and is valid only for the valence bands. The matrix elements are given by

$$\begin{aligned} F &= \Delta_1 + \Delta_2 + \lambda + \theta, & K &= \frac{\hbar^2}{2m_0} A_5 (k_x + ik_y)^2 + D_5 \epsilon_+, \\ G &= \Delta_1 - \Delta_2 + \lambda + \theta, & H &= \frac{\hbar^2}{2m_0} A_6 k_z (k_x + ik_y) + D_6 \epsilon_{z+}, \\ \lambda &= E_v + \frac{\hbar^2}{2m_0} [A_1 k_z^2 + A_2 (k_x^2 + k_y^2)] + \lambda_\epsilon, & \Delta &= \sqrt{2} \Delta_3, \\ \lambda_\epsilon &= D_1 \epsilon_{zz} + D_2 (\epsilon_{xx} + \epsilon_{yy}), & \Delta_1 &= \sqrt{2} \Delta_{cr}, \\ \theta &= \frac{\hbar^2}{2m_0} [A_3 k_z^2 + A_4 (k_x^2 + k_y^2)] + \theta_\epsilon, & \epsilon_{\pm} &= \epsilon_{xx} \pm 2i\epsilon_{xy} - \epsilon_{yy}, \\ \theta_\epsilon &= D_3 \epsilon_{zz} + D_4 (\epsilon_{xx} + \epsilon_{yy}), & \epsilon_{z\pm} &= \epsilon_{zx} \pm i\epsilon_{yz}. \end{aligned}$$

Here, k_x , k_y , and k_z are the corresponding components of the three-dimensional wave vector, ϵ_{ij} are the components of the strain tensor, and the rest are material parameters. In the cubic approximation, the parameters satisfy the relations

$$\begin{aligned} A_1 - A_2 &= -A_3 = 2A_4, & A_3 + 4A_5 &= \sqrt{2}A_6, & \Delta_2 &= \Delta_3 = \frac{1}{3}\Delta_{so}, \\ D_1 - D_2 &= -D_3 = 2D_4, & D_3 + 4D_5 &= \sqrt{2}D_6. \end{aligned}$$

For a quantum well the component k_z is replaced by the derivative $-i\frac{\partial}{\partial z}$ and the resulting one-dimensional Schrödinger equation is solved for every two-dimensional wavevector $\mathbf{k} = (k_x, k_y)$. The nonvanishing components of the strain tensor inside the quantum well are given by [41]

$$\epsilon_{xx} = \epsilon_{yy} = \frac{a_0 - a}{a}, \quad \epsilon_{zz} = -\frac{2C_{13}}{C_{33}}\epsilon_{xx},$$

where C_{ij} are the components of the elasticity tensor, a_0 is the lattice constant of the surrounding material and a is the lattice constant of the quantum well. Since the band gap of the quantum film material is smaller than that of the surrounding materials, the question of aligning the band edges for

electrons and holes remains. If E_G^0 is the band gap of the substrate and E_G is the band gap of the quantum film material, the energies at the Γ -point are modified as follows:

$$\begin{aligned} E_c &= E_c^0 - (E_G^0 - E_G)\eta, \\ E_v &= E_v^0 + (E_G^0 - E_G)(1 - \eta). \end{aligned}$$

The parameter η is set to $\frac{2}{3}$ [41]. For the conduction band the Hamiltonian is given by

$$\hat{H}^e = E_c + \Delta_1 + \Delta_2 + P_{ce} + \frac{\hbar^2}{2m_e^z} k_z^2 + \frac{\hbar^2}{2m_e^p} (k_x^2 + k_y^2), \quad (25)$$

$$P_{ce} = a_{cz}\epsilon_{zz} + a_{ct}(\epsilon_{xx} + \epsilon_{yy}). \quad (26)$$

The material parameters m_e^z and m_e^p are the effective masses of the conduction band in the z -direction and perpendicular directions, respectively. The parameters a_{cz} and a_{ct} determine the shift of the band edge due to material strain. In comparison to many other crystal structures, such as the zinc blende structure, the effect of piezoelectricity must be additionally considered in wurtzite crystals [45]. Due to the strain of the material within the quantum film, a polarization is generated, which is determined by the corresponding piezoelectric constants [42]:

$$P(z) = P_{sp} + 2d_{13} \left(C_{11} + C_{12} - \frac{2C_{13}}{C_{33}} \right) \epsilon_{xx}.$$

In addition to the components of the elasticity tensor, two other material parameters, P_{sp} and d_{13} , come into play. The polarization within the quantum film differs from that of the surrounding material, resulting in charges at the interfaces between the materials:

$$\rho(z) = \frac{\partial}{\partial z} P(z).$$

A solution of the Poisson equation [46] given by:

$$\frac{\partial}{\partial z} \left(\epsilon_s(z) \frac{\partial}{\partial z} \phi(z) \right) = -\frac{\rho(z)}{\epsilon_0}$$

provides an electrostatic potential that modifies the band edges as follows:

$$\begin{aligned} E'_c(z) &= E_c - e\phi(z) \\ E'_v(z) &= E_v - e\phi(z). \end{aligned}$$

The charge carriers in the quantum film align accordingly, thereby weakening the field within the quantum film. To account for this effect, an assumption regarding the distribution function of the charge carriers is required. Here, a Fermi-Dirac distribution is used, where the temperature and the charge carrier density n_0 are given. The chemical potential must be chosen such that the following holds:

$$\begin{aligned} n_e &= n_0 = \frac{2}{A} \sum_{\mathbf{k}} \frac{1}{e^{\beta(\epsilon_{\mathbf{k}}^e - \mu_e)} + 1} = \frac{2}{A} \sum_{\mathbf{k}} f_{\mathbf{k}}^{e,FD}, \\ n_h &= n_0 = \frac{1}{A} \sum_{\lambda\mathbf{k}} \frac{1}{e^{\beta(\epsilon_{\lambda\mathbf{k}}^h - \mu_h)} + 1} = \frac{2}{A} \sum_{\lambda\mathbf{k}} f_{\mathbf{k}}^{\lambda,FD}. \end{aligned}$$

The double degeneracy due to spin has been taken into account by the factor of 2 for the conduction band electrons. In the Poisson equation, the additional charge density $\rho_{QW}(z)$ needs to be considered, which satisfies:

$$\rho_{QW}(z) = \rho_e(z) + \rho_h(z), \quad \rho_e(z) = -\frac{2e}{A} \sum_{\mathbf{k}} |\xi_{\mathbf{k}}^e(z)|^2 f_{\mathbf{k}}^{e,FD}, \quad \rho_h(z) = \frac{e}{A} \sum_{\lambda\alpha\mathbf{k}} |\xi_{\lambda\alpha\mathbf{k}}^h(z)|^2 f_{\mathbf{k}}^{\lambda,FD}.$$

Here, $\xi_{\mathbf{k}}^e$ and $\xi_{\lambda\alpha\mathbf{k}}^h$ are eigenfunctions of the Hamiltonian operators from equations (24) and (26), and $\varepsilon_{\mathbf{k}}^e$ and $\varepsilon_{\mathbf{k}}^h$ correspond to their respective eigenvalues. However, since the Hamiltonian operator depends on the electrostatic potential, the entire problem must be solved self-consistently.

Regarding the boundary conditions, in the Schrödinger equation, the condition $\xi(z=0) = \xi(z=L_Z) = 0$ is simply assumed, where L_Z is the length of the simulation cell. For the Poisson equation, the Neumann boundary conditions $\frac{\partial\phi(z=0)}{\partial z} = \frac{\partial\phi(z=L_Z)}{\partial z} = 0$ are used. By imposing these conditions, the solution of the Poisson equation becomes independent of the length of the simulation cell.

For the TE polarized modes the optical matrix elements are given by

$$S_{\lambda\alpha} = \int dz (\xi_{\mathbf{k}}^e(z))^* \xi_{\lambda\alpha\mathbf{k}}^h(z),$$

$$|p_{\lambda}^{\text{TE}}|^2 = \frac{|p_x|^2}{2} [|S_{\lambda 1}|^2 + |S_{\lambda 2}|^2 + |S_{\lambda 4}|^2 + |S_{\lambda 5}|^2].$$

All the parameters used in the $\mathbf{k} \cdot \mathbf{p}$ calculations are given in table 1 and are taken from Ref. [43]. The temperature dependent band gap is calculated using

$$E_G = E_G^0 - \alpha \frac{T^2}{T + \beta}$$

The $\mathbf{k} \cdot \mathbf{p}$ wavefunctions and bandstructure are shown in Fig. 6 for the parameters used in the mode dynamics calculations.

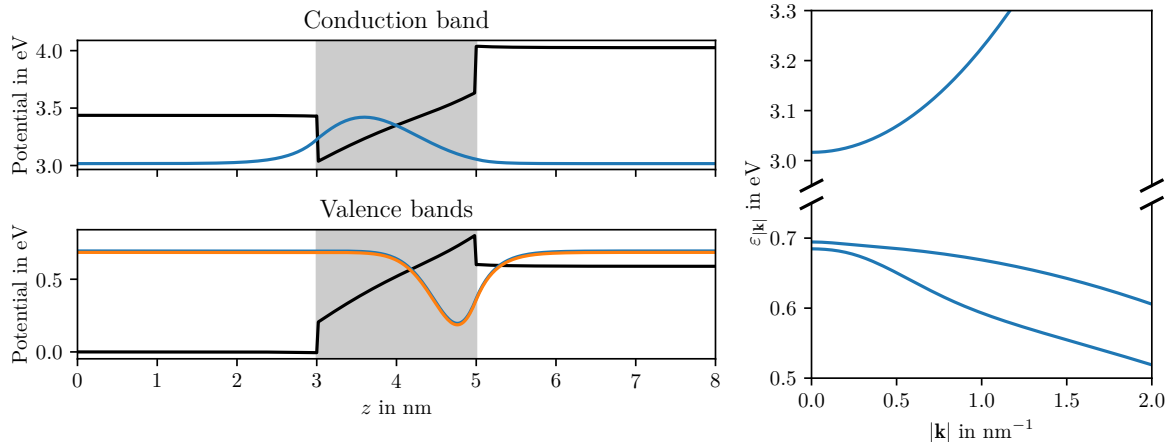


Figure 6: Calculation of the band structure of an InGaN quantum with a thickness of 2 nm and an indium concentration of 28 %. The wavefunctions of the conduction band and the first two valence bands at the Γ point are shown in the figure on the left together with the potential. The grey area illustrates the position of the quantum well. The $\mathbf{k} \cdot \mathbf{p}$ band structure is presented on the right for these three bands.

B Scattering terms for the Coulomb Interaction

The contribution due to Coulomb scattering to the equations of motion of the distribution function is given by [39, 47]

$$\begin{aligned} \left. \frac{d}{dt} f_{\mathbf{k}}^{\lambda} \right|_{\text{Coulomb}} &= \frac{4\pi}{A^2 \hbar} \sum_{\lambda' \mathbf{q} \mathbf{k}'} \left| W_{\mathbf{q}}^{\lambda \lambda'} \left((\varepsilon_{\mathbf{k}+\mathbf{q}}^{\lambda} - \varepsilon_{\mathbf{k}}^{\lambda}) / \hbar \right) \right|^2 \delta \left(\varepsilon_{\mathbf{k}+\mathbf{q}}^{\lambda} - \varepsilon_{\mathbf{k}}^{\lambda} - \varepsilon_{\mathbf{k}'+\mathbf{q}}^{\lambda'} + \varepsilon_{\mathbf{k}'}^{\lambda'} \right) \\ &\times \left[(1 - f_{\mathbf{k}}^{\lambda}) f_{\mathbf{k}+\mathbf{q}}^{\lambda} (1 - f_{\mathbf{k}'+\mathbf{q}}^{\lambda'}) f_{\mathbf{k}'}^{\lambda'} - f_{\mathbf{k}}^{\lambda} (1 - f_{\mathbf{k}+\mathbf{q}}^{\lambda}) f_{\mathbf{k}'+\mathbf{q}}^{\lambda'} (1 - f_{\mathbf{k}'}^{\lambda'}) \right], \end{aligned} \quad (27)$$

where $W_{\mathbf{q}}^{\lambda \lambda'}(\omega)$ is the screened Coulomb interaction

$$W_{\mathbf{q}}^{\lambda \lambda'}(\omega) = V_{\mathbf{q}}^{\lambda \lambda'} + \sum_{\lambda''} V_{\mathbf{q}}^{\lambda \lambda''} P_{\mathbf{q}}^{\lambda''}(\omega) W_{\mathbf{q}}^{\lambda'' \lambda'}(\omega).$$

The polarization is given by the Lindhard formula [39, 44]:

$$P_{\mathbf{q}}^{\lambda}(\omega) = \frac{2}{A} \sum_{\mathbf{k}} \frac{f_{\mathbf{k}+\mathbf{q}}^{\lambda} - f_{\mathbf{k}}^{\lambda}}{\hbar \omega - \varepsilon_{\mathbf{k}}^{\lambda} + \varepsilon_{\mathbf{k}+\mathbf{q}}^{\lambda} + i \delta_{\text{W}}}.$$

Substituting $f_{\mathbf{k}}^{\lambda} = f_{\mathbf{k}}^{\lambda, \text{FD}} + \delta f_{\mathbf{k}}^{\lambda}$ into Eq. (27) and only considering terms up to first order in $\delta f_{\mathbf{k}}^{\lambda}$ yields Eq. (7) with the scattering matrix

$$\begin{aligned} J_{\mathbf{k}, \mathbf{k}+\mathbf{q}}^{\lambda} &= - \frac{4\pi}{A^2 \hbar} \sum_{\lambda' \mathbf{k}'} \left| W_{\mathbf{q}}^{\lambda \lambda'} \left((\varepsilon_{\mathbf{k}+\mathbf{q}}^{\lambda} - \varepsilon_{\mathbf{k}}^{\lambda}) / \hbar \right) \right|^2 \delta \left(\varepsilon_{\mathbf{k}+\mathbf{q}}^{\lambda} - \varepsilon_{\mathbf{k}}^{\lambda} - \varepsilon_{\mathbf{k}'+\mathbf{q}}^{\lambda'} + \varepsilon_{\mathbf{k}'}^{\lambda'} \right) \\ &\times \left[(1 - f_{\mathbf{k}}^{\lambda}) (1 - f_{\mathbf{k}'+\mathbf{q}}^{\lambda'}) f_{\mathbf{k}'}^{\lambda'} + f_{\mathbf{k}}^{\lambda} f_{\mathbf{k}'+\mathbf{q}}^{\lambda'} (1 - f_{\mathbf{k}'}^{\lambda'}) \right] \\ &+ \delta_{\mathbf{k}, \mathbf{k}+\mathbf{q}} \frac{4\pi}{A^2 \hbar} \sum_{\lambda' \mathbf{k}' \mathbf{q}'} \left| W_{\mathbf{q}'}^{\lambda \lambda'} \left((\varepsilon_{\mathbf{k}+\mathbf{q}'}^{\lambda} - \varepsilon_{\mathbf{k}}^{\lambda}) / \hbar \right) \right|^2 \delta \left(\varepsilon_{\mathbf{k}+\mathbf{q}'}^{\lambda} - \varepsilon_{\mathbf{k}}^{\lambda} - \varepsilon_{\mathbf{k}'+\mathbf{q}'}^{\lambda'} + \varepsilon_{\mathbf{k}'}^{\lambda'} \right) \\ &\times \left[f_{\mathbf{k}+\mathbf{q}'}^{\lambda} (1 - f_{\mathbf{k}'+\mathbf{q}'}^{\lambda'}) f_{\mathbf{k}'}^{\lambda'} + (1 - f_{\mathbf{k}+\mathbf{q}'}^{\lambda}) f_{\mathbf{k}'+\mathbf{q}'}^{\lambda'} (1 - f_{\mathbf{k}'}^{\lambda'}) \right]. \end{aligned}$$

For the microscopic polarizations the dephasing term is given by [39, 47]

$$\begin{aligned} \left. \frac{d}{dt} \psi_{\mathbf{k}}^{\lambda} \right|_{\text{Coulomb}} &= \frac{2}{A^2 \hbar} \sum_{\substack{\mathbf{q} \mathbf{k}' \\ \lambda' \lambda'' \in \{e, \lambda\}}} \left| W_{\mathbf{q}}^{\lambda' \lambda''} \left((\varepsilon_{\mathbf{k}'+\mathbf{q}}^{\lambda''} - \varepsilon_{\mathbf{k}'}^{\lambda''}) / \hbar \right) \right|^2 \\ &\times \left[g \left(\varepsilon_{\mathbf{k}+\mathbf{q}}^{\lambda'} - \varepsilon_{\mathbf{k}}^{\lambda'} - \varepsilon_{\mathbf{k}'+\mathbf{q}}^{\lambda''} + \varepsilon_{\mathbf{k}'}^{\lambda''} \right) \psi_{\mathbf{k}+\mathbf{q}}^{\lambda} \right. \\ &\quad \times \left[(1 - f_{\mathbf{k}}^{\lambda'}) (1 - f_{\mathbf{k}'+\mathbf{q}}^{\lambda''}) f_{\mathbf{k}'}^{\lambda''} + f_{\mathbf{k}}^{\lambda'} f_{\mathbf{k}'+\mathbf{q}}^{\lambda''} (1 - f_{\mathbf{k}'}^{\lambda''}) \right] \\ &\quad - g \left(\varepsilon_{\mathbf{k}}^{\lambda'} - \varepsilon_{\mathbf{k}+\mathbf{q}}^{\lambda'} - \varepsilon_{\mathbf{k}'}^{\lambda''} + \varepsilon_{\mathbf{k}'+\mathbf{q}}^{\lambda''} \right) \psi_{\mathbf{k}}^{\lambda} \\ &\quad \left. \times \left[f_{\mathbf{k}+\mathbf{q}}^{\lambda'} (1 - f_{\mathbf{k}'+\mathbf{q}}^{\lambda''}) f_{\mathbf{k}'}^{\lambda''} + (1 - f_{\mathbf{k}+\mathbf{q}}^{\lambda'}) f_{\mathbf{k}'+\mathbf{q}}^{\lambda''} (1 - f_{\mathbf{k}'}^{\lambda''}) \right] \right], \end{aligned}$$

where

$$g(x) = \frac{i}{x + i\delta}.$$

For Coulomb scattering the dephasing matrix in Eq. (3) is therefore given by

$$\begin{aligned} \Gamma_{\mathbf{k},\mathbf{k}+\mathbf{q}}^\lambda = & -\frac{2}{A^2} \sum_{\substack{\mathbf{k}' \\ \lambda'\lambda'' \in \{e,\lambda\}}} \left| W_{\mathbf{q}}^{\lambda'\lambda''} \left(\left(\varepsilon_{\mathbf{k}'+\mathbf{q}}^{\lambda'} - \varepsilon_{\mathbf{k}'}^{\lambda''} \right) / \hbar \right) \right|^2 \left[g \left(\varepsilon_{\mathbf{k}+\mathbf{q}}^{\lambda'} - \varepsilon_{\mathbf{k}}^{\lambda'} - \varepsilon_{\mathbf{k}'+\mathbf{q}}^{\lambda''} + \varepsilon_{\mathbf{k}'}^{\lambda''} \right) \right. \\ & \times \left. \left[(1 - f_{\mathbf{k}}^{\lambda'}) (1 - f_{\mathbf{k}'+\mathbf{q}}^{\lambda''}) f_{\mathbf{k}'}^{\lambda''} + f_{\mathbf{k}}^{\lambda'} f_{\mathbf{k}'+\mathbf{q}}^{\lambda''} (1 - f_{\mathbf{k}'}^{\lambda''}) \right] \right] \\ & + \delta_{\mathbf{k},\mathbf{k}+\mathbf{q}} \frac{2}{A^2} \sum_{\substack{\mathbf{q}'\mathbf{k}' \\ \lambda'\lambda'' \in \{e,\lambda\}}} \left| W_{\mathbf{q}'}^{\lambda'\lambda''} \left(\left(\varepsilon_{\mathbf{k}'+\mathbf{q}'}^{\lambda'} - \varepsilon_{\mathbf{k}'}^{\lambda''} \right) / \hbar \right) \right|^2 \left[g \left(\varepsilon_{\mathbf{k}}^{\lambda'} - \varepsilon_{\mathbf{k}+\mathbf{q}'}^{\lambda'} - \varepsilon_{\mathbf{k}'}^{\lambda''} + \varepsilon_{\mathbf{k}'+\mathbf{q}'}^{\lambda''} \right) \right. \\ & \times \left. \left[f_{\mathbf{k}+\mathbf{q}'}^{\lambda'} (1 - f_{\mathbf{k}'+\mathbf{q}'}^{\lambda''}) f_{\mathbf{k}'}^{\lambda''} + (1 - f_{\mathbf{k}+\mathbf{q}'}^{\lambda'}) f_{\mathbf{k}'+\mathbf{q}'}^{\lambda''} (1 - f_{\mathbf{k}'}^{\lambda''}) \right] \right]. \end{aligned}$$

C Equations of Motion

The equation of motion for the electron density is given by [20]

$$\frac{d}{dt} n_e = \frac{d}{dt} \frac{2}{A} \sum_{\mathbf{k}} f_{\mathbf{k}}^e = \sum_p \omega_p S_p |u_p(\mathbf{r}_{\parallel})|^2 \text{Im} \chi(\omega_p) - \frac{n_e}{\tau_{\text{nr}}} - \sum_{\lambda} \frac{2}{A} \sum_{\mathbf{k}} B_{\mathbf{k}}^{\lambda} f_{\mathbf{k}}^e f_{\mathbf{k}}^{\lambda} + \frac{j \eta_{\text{inj}}}{e},$$

analogous for the hole density. They can be derived from Eq. (15) assuming Fermi-Dirac distributions for the carriers, except for the spontaneous emission term and the pump term. The quantum wells are pumped by a current density j which is assumed to be the same for both electrons and holes. The prefactor $B_{\mathbf{k}}^{\lambda}$ in the spontaneous emission term is given by

$$B_{\mathbf{k}}^{\lambda} = C_{\lambda} \frac{2n_{\text{eff}}^3}{3\pi c^3 \hbar^2} (\varepsilon_{\mathbf{k}}^e + \varepsilon_{\mathbf{k}}^{\lambda})$$

and can also be found in Ref. [19] in a similar form. In the simulations the carrier density is assumed to be constant directly under the ridge, therefore this equation is averaged over the ridge area:

$$\frac{d}{dt} n_e = \sum_p \omega_p S_p \text{Im} \chi(\omega_p) \frac{1}{Lw_r} \int_0^{w_r} dx \int_0^L dy |u_p(\mathbf{r}_{\parallel})|^2 - \frac{n_e}{\tau_{\text{nr}}} - \sum_{\lambda} \frac{2}{A} \sum_{\mathbf{k}} B_{\mathbf{k}}^{\lambda} f_{\mathbf{k}}^e f_{\mathbf{k}}^{\lambda} + \frac{I \eta_{\text{inj}}}{eLw_r},$$

where I is the current and w_r is the ridge width. The equation of motion for the photon numbers is given by Eq. (11) and Eq. (14), with an additional spontaneous emission term and a loss term determined by the photon lifetime τ_{photon} :

$$\begin{aligned} \frac{d}{dt} S_p = & S_p \omega_p \int_0^{w_r} dx \int_0^L dy |u_p(\mathbf{r}_{\parallel})|^2 \text{Im} \chi(\omega_p) + \int d^2 \mathbf{r}_{\parallel} |u_p(\mathbf{r}_{\parallel})|^2 I_{\text{SE}}(\omega_p, \mathbf{r}_{\parallel}) \\ & + \sum_{q \neq p} \frac{S_p S_q}{\omega_p \omega_q} \int d^2 \mathbf{r}_{\parallel} |u_p(\mathbf{r}_{\parallel})|^2 |u_q(\mathbf{r}_{\parallel})|^2 A(\omega_q - \omega_p, \mathbf{r}_{\parallel}) - \frac{S_p}{\tau_{\text{photon}}}. \end{aligned}$$

The spontaneous emission spectrum is calculated like the gain spectrum, except that the factor $1 - f_{\mathbf{k}}^e - f_{\mathbf{k}}^{\lambda}$ is replaced by $f_{\mathbf{k}}^e f_{\mathbf{k}}^{\lambda}$:

$$I_{\text{SE}}(\omega) = -\frac{2}{A} \sum_{\lambda \mathbf{k}} \frac{C_{\lambda}}{\omega} \text{Im} \left\{ \sum_{\mathbf{k}'} \Lambda_{\mathbf{k}\mathbf{k}'}^{\lambda,-1}(\omega) f_{\mathbf{k}'}^e f_{\mathbf{k}'}^{\lambda} \right\}.$$

In the simulation we consider different longitudinal modes as standing waves and only the fundamental lateral TE mode, which is approximated by a sine function [11]:

$$\mathbf{u}_p(\mathbf{r}) = \mathbf{e}_x Z(z) \sqrt{\frac{2}{L}} \sin\left(\frac{\pi p}{L} y\right) \sqrt{\frac{2}{w_r}} \sin\left(\frac{\pi}{w_r} x\right).$$

In this case the equations of motion are given by

$$\begin{aligned} \frac{d}{dt} n_e &= \sum_p \frac{C \omega_p S_p}{L w_r} \text{Im} \chi(\omega_p) - \frac{n_e}{\tau_{nr}} - \sum_\lambda \frac{2}{A} \sum_{\mathbf{k}} B_{\mathbf{k}}^\lambda f_{\mathbf{k}}^e f_{\mathbf{k}}^\lambda + \frac{I \eta_{inj}}{e L w_r}, \\ \frac{d}{dt} S_p &= S_p \omega_p C \text{Im} \chi(\omega_p) + C I_{SE}(\omega_p) + \sum_{q \neq p} \frac{S_p S_q}{\omega_p \omega_q} \frac{3}{2} C^2 A(\omega_q - \omega_p) - \frac{S_p}{\tau_{photon}}. \end{aligned}$$

where the constant C is related to the confinement factor ξ :

$$C = |Z(z_{QW})|^2 \approx \frac{\xi}{n_{\text{eff}}^2 d_{QW}}.$$

The spacing of the mode frequencies is determined by the refractive group index n_{gr} and the frequency of the mode with index p is given by

$$\omega_p = \frac{\pi n_{\text{eff}}}{L c} p_0 + (p - p_0) \frac{\pi n_{gr}}{L c}.$$

The integer p_0 is determined by

$$p_0 = \text{round}\left(\frac{\omega_0 L c}{\pi n_{\text{eff}}}\right)$$

where the frequency ω_0 is the gain maximum and c is the speed of light in vacuum.

Table 1: $\mathbf{k} \cdot \mathbf{p}$ parameters for GaN and InN, taken from Ref. [43]. In addition there are bowing parameters for the band gap $b_{E_G^0} = 1400$ meV and the polarization $b_{P_{sp}} = -0.037$ Cm⁻², also taken from Ref. [43].

		GaN	InN
a	Lattice constant	0.3189 nm	0.3545 nm
c	Lattice constant	0.5185 nm	0.5703 nm
m_e^z	Perpendicular electron effective mass	$0.2 m_0$	$0.07 m_0$
m_e^p	Parallel electron effective mass	$0.21 m_0$	$0.07 m_0$
A_1		-7.21	-8.21
A_2		-0.44	-0.68
A_3		6.68	7.57
A_4		-3.46	-5.23
A_5		-3.4	-5.11
A_6		-4.9	-5.96
Δ_{cr}		10 meV	24 meV
Δ_{so}		17 meV	5 meV
$E_{px} = E_{pz} = E_p$	Optical matrix element	19.8 eV	11.4 eV
E_G^0	Band gap	3510 meV	690 meV
α	Band gap parameter	0.914 meVK^{-1}	0.414 meVK^{-1}
β	Band gap parameter	825 K	154 K
ϵ_s	Static dielectric constant	9.7	14.4
D_1		-3.6 eV	-3.6 eV
D_2		1.7 eV	1.7 eV
D_3		5.2 eV	5.2 eV
D_4		-2.7 eV	-2.7 eV
D_5		-2.8 eV	-2.8 eV
D_6		-4.3 eV	-4.3 eV
a_{cz}		-7.1 eV	-4.2 eV
a_{ct}		-9.9 eV	-4.2 eV
d_{13}		-1.0 pmV^{-1}	-3.5 pmV^{-1}
d_{33}		1.9 pmV^{-1}	7.6 pmV^{-1}
P_{sp}		-0.034 Cm^{-2}	-0.042 Cm^{-2}
C_{11}		390 GPa	223 GPa
C_{12}		145 GPa	115 GPa
C_{13}		106 GPa	92 GPa
C_{33}		398 GPa	224 GPa